

Diagnosing observation error correlations for Doppler radar radial winds in the Met Office UKV model using observation-minus-background and observation-minus-analysis statistics

Article

Published Version

Creative Commons: Attribution 4.0 (CC-BY)

Open Access

Waller, J. A., Simonin, D., Dance, S. L. ORCID: <https://orcid.org/0000-0003-1690-3338>, Nichols, N. K. ORCID: <https://orcid.org/0000-0003-1133-5220> and Ballard, S. P. (2016) Diagnosing observation error correlations for Doppler radar radial winds in the Met Office UKV model using observation-minus-background and observation-minus-analysis statistics. *Monthly Weather Review*, 144 (10). pp. 3533-3551. ISSN 0027-0644 doi: 10.1175/MWR-D-15-0340.1 Available at <https://centaur.reading.ac.uk/65806/>

It is advisable to refer to the publisher's version if you intend to cite from the work. See [Guidance on citing](#).

To link to this article DOI: <http://dx.doi.org/10.1175/MWR-D-15-0340.1>

Publisher: American Meteorological Society

All outputs in CentAUR are protected by Intellectual Property Rights law, including copyright law. Copyright and IPR is retained by the creators or other copyright holders. Terms and conditions for use of this material are defined in the [End User Agreement](#).

www.reading.ac.uk/centaur

CentAUR

Central Archive at the University of Reading

Reading's research outputs online

Diagnosing Observation Error Correlations for Doppler Radar Radial Winds in the Met Office UKV Model Using Observation-Minus-Background and Observation-Minus-Analysis Statistics

J. A. WALLER

School of Mathematical and Physical Sciences, University of Reading, Reading, United Kingdom

D. SIMONIN

MetOffice@Reading, University of Reading, Reading, United Kingdom

S. L. DANCE AND N. K. NICHOLS

School of Mathematical and Physical Sciences, University of Reading, Reading, United Kingdom

S. P. BALLARD

MetOffice@Reading, University of Reading, Reading, United Kingdom

(Manuscript received 3 September 2015, in final form 7 June 2016)


ABSTRACT

With the development of convection-permitting numerical weather prediction the efficient use of high-resolution observations in data assimilation is becoming increasingly important. The operational assimilation of these observations, such as Doppler radar radial winds (DRWs), is now common, although to avoid violating the assumption of uncorrelated observation errors the observation density is severely reduced. To improve the quantity of observations used and the impact that they have on the forecast requires the introduction of the full, potentially correlated, error statistics. In this work, observation error statistics are calculated for the DRWs that are assimilated into the Met Office high-resolution U.K. model (UKV) using a diagnostic that makes use of statistical averages of observation-minus-background and observation-minus-analysis residuals. This is the first in-depth study using the diagnostic to estimate both horizontal and along-beam observation error statistics. The new results obtained show that the DRW error standard deviations are similar to those used operationally and increase as the observation height increases. Surprisingly, the estimated observation error correlation length scales are longer than the operational thinning distance. They are dependent both on the height of the observation and on the distance of the observation away from the radar. Further tests show that the long correlations cannot be attributed to the background error covariance matrix used in the assimilation, although they are, in part, a result of using superobservations and a simplified observation operator. The inclusion of correlated error statistics in the assimilation allows less thinning of the data and hence better use of the high-resolution observations.

1. Introduction

With the recent development of convection-permitting numerical weather prediction (NWP), such as the Met Office U.K. variable resolution (UKV) model ([Lean et al.](#)

[2008](#); [Tang et al. 2013](#)), the assimilation of observations that have high frequency both in space and time has become increasingly important ([Park and Zupanski 2003](#); [Dance 2004](#); [Sun et al. 2014](#); [Ballard et al. 2016](#); [Clark et al. 2015](#)). The potential for assimilating one such set of observations, the Doppler radar radial winds (DRWs) ([Lindskog et al. 2004](#); [Sun 2005](#)), has been explored by a number of operational centers (e.g., [Lindskog et al. 2001](#); [Salonen et al. 2007](#); [Rihan et al. 2008](#); [Salonen et al. 2009](#)). The assimilation of the DRWs has been shown to provide a significant positive impact on the forecast ([Xiao et al. 2005](#); [Lindskog et al. 2004](#); [Montmerle and Faccani](#)

 Denotes Open Access content.

Corresponding author address: J. A. Waller, Department of Meteorology, University of Reading, Earley Gate, P.O. Box 243, Reading, RG6 6BB, United Kingdom.
E-mail: j.a.waller@reading.ac.uk

DOI: 10.1175/MWR-D-15-0340.1

2009; Simonin et al. 2014; Xue et al. 2013, 2014) and as a result they are now included in operational assimilation (Xiao et al. 2008; Simonin et al. 2014).

Currently at the Met Office the error statistics associated with DRWs are assumed to be uncorrelated (Simonin et al. 2014). To reduce the large quantity of data and ensure the assumption of uncorrelated errors is reasonable the DRW observations are “superobbed” and thinned before assimilation (Simonin et al. 2014). These processes result in a large number of observations being discarded. To improve convection-permitting NWP it is necessary to make better use of high-frequency DRW observations. This requires less thinning of the observational data, and hence the inclusion of correlated observation error statistics in the assimilation system is required (Liu and Rabier 2003). Currently the full observation error statistics associated with the DRWs are unknown. Therefore, the aim of this manuscript is both to estimate and to provide an understanding of the correlated observation errors associated with DRW.

In general, the errors associated with the observations can be attributed to four main sources: 1) instrument error, 2) error introduced in the observation operator, 3) errors of “representativity” (i.e., errors that arise where the observations can resolve spatial scales that the model cannot), and 4) preprocessing errors (i.e., errors introduced by preprocessing). For DRWs the instrument errors are independent and uncorrelated. Observation error correlations, which may be state dependent and dependent on the model resolution, are likely to arise from the other sources of error (Janjić and Cohn 2006; Waller 2013; Waller et al. 2014a,b) (see section 5b for a more detailed description). The inclusion of correlated observation errors in the assimilation has been shown to lead to a more accurate analysis, the inclusion of more observation information content, and improvements in the forecast skill score (Stewart et al. 2013; Stewart 2010; Healy and White 2005; Stewart et al. 2008; Weston et al. 2014). Significant benefit may even be provided by using only a crude approximation to the observation error covariance matrix (Stewart et al. 2013; Healy and White 2005).

A number of methods exist for estimating the observation error covariances (e.g., Hollingsworth and Lönnberg 1986; Dee and da Silva 1999). Xu et al. (2007) presented an innovation method based on that of Hollingsworth and Lönnberg (1986) for estimating DRW error and background wind error covariances. Simonin et al. (2012) previously calculated observation error statistics for DRWs using the method of Xu et al. (2007). The work of Simonin et al. (2012) suggests that the observation error standard deviation increases with the height of the observation and that the observations

errors have a correlation length scale of 1–3 km. However, the Hollingsworth and Lönnberg (1986) method was initially designed to provide estimates of the background error statistics under the assumption of uncorrelated observation errors. The method can be used to estimate both correlated background and correlated observation errors; however, determining how to split the estimated quantity into observation and background errors is nontrivial (Bormann and Bauer 2010). Indeed the result is subjective. To overcome this difficulty most recent attempts to diagnose the observation error correlations have made use of the diagnostic proposed in Desroziers et al. (2005). Initially designed as a consistency check, the diagnostic provides an estimate of the observation error covariance matrix using the statistical average of observation-minus-background and observation-minus-analysis residuals. However, in theory it relies on the use of exact background and observation error statistics in the assimilation. Despite this limitation, the diagnostic has been used to estimate interchannel observation error statistics (Stewart et al. 2009, 2014; Bormann and Bauer 2010; Bormann et al. 2010; Weston et al. 2014) even when the error statistics used in the assimilation are not exact. The method of Desroziers et al. (2005) has also been used by Wattrelot et al. (2012) to calculate observation error statistics for the Doppler radial winds assimilated into the Météo-France system. Their results, published as a conference paper, show a similar error standard deviation to those found in Simonin et al. (2012), but suggest that the observation errors have a larger correlation length scale of approximately 10 km (we cannot determine the length scale precisely because of the data thinning they have applied).

Here we present the first in-depth study using the diagnostic of Desroziers et al. (2005) to calculate observation error statistics for the DRWs assimilated into the Met Office UKV model. Because of the limitations of the diagnostic we consider the sensitivity of the estimated observation error statistics to the choice of assimilated background error statistics. To aid our understanding of the source of observation error we also consider the sensitivity of the estimated observation error statistics to the use of superobservations and the use of a more sophisticated observation operator. We find that, for summer season observations, the DRW error standard deviations are similar to those used operationally although, surprisingly, the observation error correlation length scales are longer than the operational thinning distance. Because of the uncertainty in the results arising from the diagnostic the estimated correlation length scales should be interpreted as indicative, rather than necessarily quantitatively perfect. However, results from the diagnostics can still provide useful information as further tests show that the long correlations

cannot be attributed to the background error covariance matrix used in the assimilation, although they may, in part, be a result of using superobservations and a simplified observation operator.

This paper is organized as follows. In [section 2](#) we give a description of the diagnostic of [Desroziers et al. \(2005\)](#). We describe the DRW observations and their model representations in [section 3](#) and in [section 4](#) we describe the experimental design. In [section 5](#) we consider the estimated observation error statistics from four different cases. Finally we conclude in [section 6](#).

2. The diagnostic of Desroziers et al. (2005)

Data assimilation techniques combine observations $\mathbf{y} \in \mathbb{R}^{N^p}$ with a model prediction of the state, the background $\mathbf{x}^b \in \mathbb{R}^{N^m}$, often determined by a previous forecast. Here N^p and N^m denote the dimensions of the observation and model state vectors, respectively. In the assimilation the observations and background are weighted by their respective errors, using the background and observation error covariance matrices $\mathbf{B} \in \mathbb{R}^{N^m \times N^m}$ and $\mathbf{R} \in \mathbb{R}^{N^p \times N^p}$, to provide a best estimate of the state, $\mathbf{x}^a \in \mathbb{R}^{N^m}$, known as the analysis. To calculate the analysis the background must be projected into the observation space using the possibly nonlinear observation operator, $\mathcal{H}: \mathbb{R}^{N^m} \rightarrow \mathbb{R}^{N^p}$. After an assimilation step the analysis is evolved forward in time to provide a background for the next assimilation.

[Desroziers et al. \(2005\)](#) assume that the analysis is determined using

$$\mathbf{x}^a = \mathbf{x}^b + \mathbf{K}[\mathbf{y} - \mathcal{H}(\mathbf{x}^b)], \quad (1)$$

where $\mathbf{K} = \mathbf{B}\mathbf{H}^T(\mathbf{H}\mathbf{B}\mathbf{H}^T + \mathbf{R})^{-1}$ is the gain matrix and \mathbf{H} is the linearized observation operator, linearized about the current state.

The diagnostic described in [Desroziers et al. \(2005\)](#) estimates the observation error covariance matrix by using the observation-minus-background and observation-minus-analysis residuals. The background residual, also known as the innovation,

$$\mathbf{d}_b^o = \mathbf{y} - \mathcal{H}(\mathbf{x}^b), \quad (2)$$

is the difference between the observation \mathbf{y} and the mapping of the forecast vector, \mathbf{x}^b , into observation space by the observation operator \mathcal{H} . The analysis residual,

$$\mathbf{d}_a^o = \mathbf{y} - \mathcal{H}(\mathbf{x}^a) \quad (3)$$

$$\approx \mathbf{y} - \mathcal{H}(\mathbf{x}^b) - \mathbf{H}\mathbf{K}\mathbf{d}_b^o, \quad (4)$$

is similar to the background residuals, but with the forecast vector replaced by the analysis vector \mathbf{x}^a . By

taking the statistical expectation of the product of the analysis and background residuals results in

$$E[\mathbf{d}_a^o \mathbf{d}_b^{oT}] \approx \mathbf{R}, \quad (5)$$

assuming that the forecast and observation errors are uncorrelated. Equation (5) is exact if the observation and background error statistics used in assimilation are exact. The theoretical work of [Waller et al. \(2016\)](#) provides insight into how results from the diagnostic can be interpreted when the incorrect background and observation error statistics are used in the assimilation. Because of the statistical nature of the diagnostic the resulting matrix will not be symmetric. Therefore, if the matrix is to be used it must be symmetrized.

3. Doppler Radar radial wind observations and their model representation

a. The Met Office UKV model and 3D variational assimilation scheme

The operational UKV model is a variable-resolution convection permitting model that covers the United Kingdom ([Lean et al. 2008](#); [Tang et al. 2013](#)). The model has 70 vertical levels. The horizontal grid has a 1.5-km fixed resolution on the interior surrounded by a variable-resolution grid that increases smoothly in size to 4 km. The variable-resolution grid allows the downscaled boundary conditions, taken from the global model, to spin up before reaching the fixed interior grid. The initial conditions are provided from a 3D variational assimilation scheme that uses an incremental approach ([Courtier et al. 1994](#)) and is a limited-area version of the Met Office variational data assimilation scheme ([Lorenc et al. 2000](#); [Rawlins et al. 2007](#)). The assimilation uses an adaptive mesh that allows the accurate representation of boundary layer structures ([Piccolo and Cullen 2011, 2012](#)). The background error covariance statistics used in this study are described in [section 4](#).

b. Doppler radar radial wind data

Doppler radar is an active remote sensing instrument that provides observations of radial wind by measuring the phase shift between a transmitted electromagnetic wave pulse and its backscatter echo. The radial velocity of a scattering target is then estimated from the Doppler shift ([Doviak and Zrnić 1993](#)). While it is possible to derive clear air radar returns (e.g., [Rennie et al. 2010, 2011](#)), in this work we consider only observations where the scattering targets are assumed to be raindrops. The DRW data used at the Met Office are acquired using 18

C-band weather radars. Each radar completes a series of scans out to a range of 100 km every 5 min at different elevation angles (typically 1°, 2°, 4°, 6°, and 9°) with a $1^\circ \times 600$ m resolution volume. Before being assimilated the data are processed and a quality control procedure is applied. This ensures that no observations that disagree with neighboring observations or have a large departure from the background are assimilated. The observations errors are assumed Gaussian and uncorrelated in space or time with standard deviations that range from 1.8 m s^{-1} for observations close to the radar to 2.8 m s^{-1} for observations farthest away from the radar. Further details of the operational assimilation of DRWs at the Met Office can be found in [Simonin et al. \(2014\)](#).

1) THE CURRENT OPERATIONAL OBSERVATION OPERATOR

To compare the background with the observations it is necessary to map the model state into observation space. The current operational observation operator, following [Lindskog et al. \(2000\)](#), first interpolates the NWP model horizontal and vertical wind components u , v , and w to the observation location. The horizontal wind is then projected in the direction of the radar beam and projected onto the slant of the radar beam using

$$v_r = (u \sin \phi + v \cos \phi) \cos(\theta) + w \sin(\theta), \quad (6)$$

where ϕ is the radar azimuth angle clockwise from due north and θ is the beam center elevation angle. The elevation angle $\theta = \varepsilon + \alpha$ includes a correction term α that must be added to the measurement elevation angle ε . The correction term

$$\alpha = \tan^{-1} \left[\frac{r \cos(\varepsilon)}{r \sin(\varepsilon) + a_e + h_r} \right], \quad (7)$$

where h_r is the height of the radar above sea level, r is the range of the observation, and a_e is the effective Earth radius (1.3 times the actual Earth radius) required to take account of Earth's curvature and the radar beam refraction ([Doviak and Zrnić 1993](#)). The correction term is not exact. The value of a_e is only valid in the international standard atmosphere. This simple operational observation operator does not account for the beam broadening or reflectivity weighting. Additionally, only the horizontal wind components are updated in the minimization, and the vertical component of wind is ignored, which for small elevation angles should be acceptable. In addition no information about hydrometeor fall speed is available to the assimilation system.

This operational observation operator is used in the majority of results discussed in this article.

2) AN IMPROVED OBSERVATION OPERATOR

An improved observation operator has been trialled in the operational system; it accounts for some broadening of the beam (vertical only), as well as a reflectivity weighting. Both of these processes are often ignored in operational DRW assimilation ([Ge et al. 2010](#)). This improved observation operator is similar to the operator described by [Xu and Wei \(2013\)](#), although it differs in some important details. The beam broadening model W_{bb} takes the form

$$W_{bb}(\theta_z) = \exp \left[-2 \ln(2) \frac{\theta_z^2}{\theta_{3\text{dB}}^2} \right], \quad (8)$$

with $\theta_z = \theta - \theta_b$, where θ is the beam center elevation as in (6), θ_b is the elevation within the beam, and $\theta_{3\text{dB}}$ is the half power bandwidth (angular range of the antenna pattern in which at least half of the maximum power is still emitted; [Toomay and Hannen 2004](#)). For the reflectivity weighting, a climatological profile with height h is used:

$$W_{\text{ref}}(h) = Zh + c, \quad (9)$$

where

$$Z = \begin{cases} -6 \text{ dB} & h < \text{Brightband}_L \\ -2 \text{ dB} & h > \text{Brightband}_U \end{cases}, \quad (10)$$

c is a constant scaling factor, Brightband_L is the lower limit of the bright band, and Brightband_U is the upper limit of the bright band. The height of the bright band (a layer of melting ice resulting in intense reflectivity return; [Kitchen 1997](#)) is derived from the forecast model temperature field, and has a thickness set to 250 m. The reflectivity profile increases by 10 dB from the bottom to the center of the bright band and then decreases linearly. The beam broadening and reflectivity weighting are combined to give a single weight, $W = W_{\text{ref}} W_{bb}$ and this weighting is included in the new observation operator:

$$v_r = \sum_{\text{ML}_{\theta_{\text{beam}}}} W(u \sin \phi + v \cos \phi) \cos(\theta). \quad (11)$$

The summation in (11) is made over the model levels ($\text{ML}_{\theta_{\text{beam}}}$) present within the beam thickness. In this formulation, $\sum W$ is equal to one over $\text{ML}_{\theta_{\text{beam}}}$. The implementation of this new observation operator has been shown to reduce the error in the background residuals. This new observation operator may be further improved ([Fabry 2010](#)), although the operational use of a more complex observation operator may not be feasible. While these simplifications and omissions in the

observation operator exist, they will introduce additional error when the model background is projected into observation space. These errors may well be correlated and should ideally be accounted for in the observation error covariance matrix.

3) SUPEROBSERVATION CREATION

To reduce the density of the observations, multiple observations are made into a single superobservation. Only observations that have passed the quality control procedure described in [Simonin et al. \(2014\)](#) are combined to make the superobservations. There are a number of methods for calculating the superobservations. The Doppler radar superobservations used at the Met Office are calculated using innovations following the method of [Salonen et al. \(2008\)](#). The radar scan is divided into 3° by 3 km cells and one observation is created per cell using the following procedure:

- 1) Project background winds into observation space using (6).
- 2) Calculate the background residual at each observation location.
- 3) Average all background residuals that fall within a superobservation cell.
- 4) Add the average residual to the simulated background radial wind at the center of the superobservation cell to give a value for the superobservation.

The calculated superobservations are subject to a second quality-control procedure ([Simonin et al. 2014](#)). They are then further thinned to 6 km, where it is assumed that the observations will have uncorrelated error, using Poisson disk sampling ([Bondarenko et al. 2007](#)).

4) SUPEROBSERVATION ERROR

The calculated superobservations have an associated superobservation error ε^{so} . The literature shows that the superobbing procedure reduces the uncorrelated portion of the error; however, the correlated error is not reduced ([Berger and Forsythe 2004](#)). [Berger and Forsythe \(2004\)](#) showed that the covariance of the superobservation error will be equivalent to the averaged observation error covariance matrix for the raw observations (i.e., creating the superobservations using the background does not introduce any background error into ε^{so}) if the following conditions are met:

- 1) The observation and background errors are independent.
- 2) The background state errors are fully correlated within the superobservation cell.
- 3) The background state errors in a superobservation cell all have the same magnitude.

- 4) The background residuals are equally weighted within a superobservation cell.

However, for DRWs it is not clear that all the assumptions will hold. In particular, assumptions 1 and 2 are valid at close range to the radar where the superobservation cells are small. However, at far range the superobservation cells are large and the assumptions are likely to be invalid. Therefore, it is possible that at large ranges there is a small influence of the background errors on the error associated with the superobservation.

5) ERROR SOURCES FOR DOPPLER RADAR RADIAL WINDS

In the introduction the four main sources of observation error are introduced. The observation error will not only be a function of the observation type, but also of the observation preprocessing, observation operator and model resolution. Here we list some of the observation error sources specific to DRWs:

- Errors introduced by clutter removal.
- Error introduced when creating the superobservations.
- Misrepresentation of radar beam bending.
- Misrepresentation of beam broadening.
- Approximation of volume measurement as point measurement.
- Discrete approximation of continuous mapping from model to observation space.
- Errors of representativity.
- Instrument error.

There may be additional unknown sources of error.

It has been shown that some of these errors, such as the instrument error or those errors caused by the misrepresentation of radar beam bending, are small ([Xu and Wei 2013](#)). However, there are other errors, such as the error introduced when creating the superobservations, misrepresentation of beam broadening, and the approximation of volume measurement as a point measurement, that we hypothesize will have a more significant contribution to the observation error statistics. Indeed, [Fabry and Kilambi \(2011\)](#) suggest that if the antenna beamwidth and reflectivity weighting are ignored in the observation operator, then the observation errors will have long correlation length scales greater than 10 km.

4. Experimental design

To calculate estimates of the observation error covariances we require background and analysis residuals. We use archived observations and background data produced by the operational Met Office system from June,

July and August 2013. To generate the analyses we run four different assimilation configurations, detailed below. Using these backgrounds, analyses, and observations we are able to determine the background \mathbf{d}_b^o and analysis \mathbf{d}_a^o residuals. Observations in this study come from 9 of the 18 radars in the network. Although observation errors are likely to be state dependent (Waller et al. 2014b), we have used 3 months' worth of data to ensure that we have enough data for the statistical sampling error to be small. We have restricted ourselves to the summer season as we expect mainly convective rainfall (Hand et al. 2004; Hawcroft et al. 2012), which is likely to result in state-dependent observation errors that are all similar.

Case 1 uses residuals produced by running the UKV under the January 2014 operational configuration. This uses superobservations (calculated as described in section 3b) thinned to 6 km and the observation operator given in (6). The background error covariance ("New") has been derived using the Covariances and VAR Transforms (CVT) software, which is the new Met Office covariance calibration and diagnostic tool that analyses training data representing forecast errors [either using the so-called National Meteorological Center (NMC) lagged forecast technique or ensemble perturbations]. Here an NMC method has been applied to $(T + 6 \text{ h}) - (T + 3 \text{ h})$ forecast differences to diagnose a variance and correlation length scale for each vertical mode.

Case 2 considers the effect of using the old (used prior to January 2013) operational UKV background error covariance matrix ("Old"). These statistics were generated from $(T + 24 \text{ h}) - (T + 12 \text{ h})$ forecast differences; contrary to the CVT approach, the correlation functions used specific fixed length scales (Ballard et al. 2016). This background error covariance matrix has larger variances than the matrix used in case 1 and the correlation length scales are slightly longer. A comparison between cases 1 and 2 shows the impact of the assimilated background error covariance matrix on the estimated observation error statistics.

Case 3 uses the same background error covariance as case 1, but used raw observations (thinned to 6 km) rather than using the superobservations. A comparison between cases 1 and 3 shows the impact of the superobservations on the estimated observation error statistics.

Case 4 uses the same design as case 3, the assimilation of raw observations, but the operational observation operator is replaced with the observation operator described in (11). A comparison between cases 3 and 4 shows the impact of the observation operator on the estimated observation error statistics.

TABLE 1. Summary of experimental design for different cases.

Case	B	Superobservations	Observation operator
1	New	Yes	Old
2	Old	Yes	Old
3	New	No	Old
4	New	No	New

We summarize the different cases in Table 1. For each case the available data for each radar scan are stored in 3D arrays of size $N^s \times N^r \times N^a$, where N^s is the number of scans containing data, $N^r = 16$ is the number of ranges, and $N^a = 120$ is the number of azimuths. Figure 1 shows a radar scan with the typical superobservation cells. The data are also separated by elevation, with data available at elevation angles 1° , 2° , 4° , and 6° . (We do not estimate the observation error statistics for the 9° beam due the lack of available data.) The position of these observations at these elevations is shown in Fig. 2 (we note that the color scheme for each given elevation is used throughout the figures in this manuscript). It is important to note that these observations are only available in areas where there is precipitation and it is possible that only part of the scan contains observations. Furthermore, the use of the superobservations, thinning, and quality control results in a limited amount of data in each scan. The amount of data available differs for each elevation, with data for the lower elevations available out to far range (a result of the quality control procedures) and for higher elevations available only for near range. This lack of data means that standard deviations and correlations are not available for every range at each elevation. Results are only plotted for standard deviations if 1500 or more samples were available and for correlations if the number of samples was greater than 500. The minimum number of samples is chosen to ensure that sampling error does not contaminate our estimates of the error statistics. Observations may be correlated along the beam, horizontally or vertically. Here we consider both horizontal correlations and those along the beam.

Horizontal correlations consider how observations at a given height are correlated. The blue cells in Fig. 1 show a set of observations that would be compared for a given height. For each radar scan, data are sorted into 200-m height bins. Here the height takes into account the height of the radar above sea level. All observations that fall into a particular height bin are considered. The data are binned by separation distance for each pair of observations and from this the correlations are calculated.

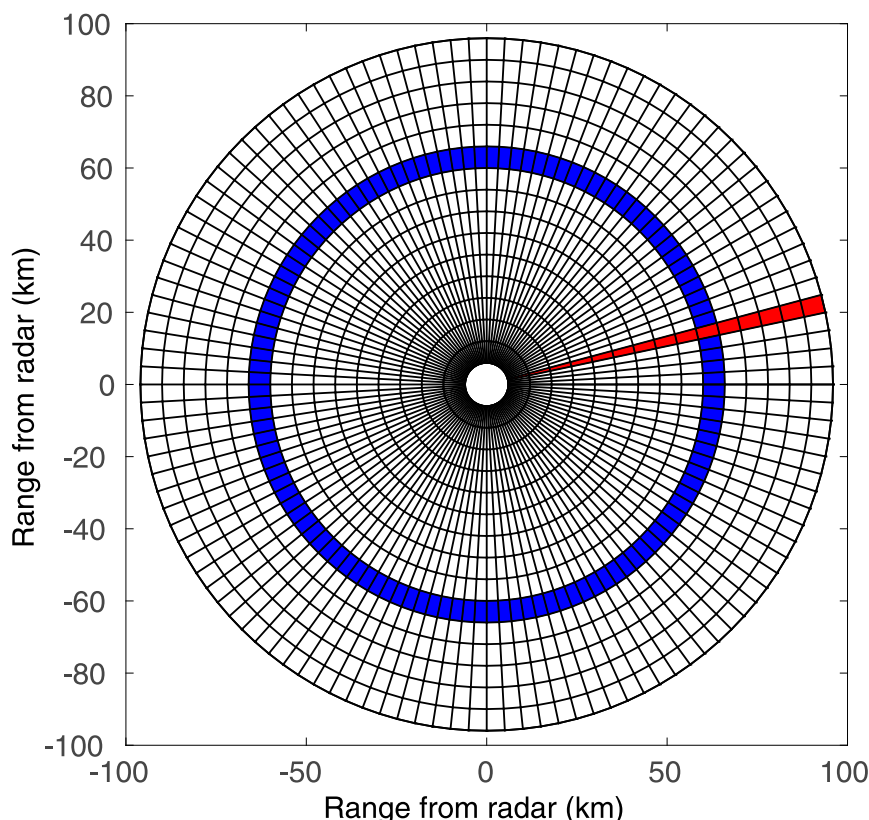


FIG. 1. A typical radar scan where each box is the location of a superobservation. The blue cells show a group of observations, all at the same height, that would be compared to calculate horizontal correlations. The red cells show observations that would be compared to calculate the along-beam correlations.

When calculating along-beam correlations we consider how observations in the same beam are correlated to each other, where correlations are expressed for the separation distance along the beam. The red cells in Fig. 1 show one set of observations that would be considered in this case. Here the samples used for calculating (5) are taken to be the individual scans along the azimuth. Samples are taken on all dates, from all radars, and from each azimuth. When calculating results along the beam we do not expect to obtain symmetric correlation functions. When considering the along-beam correlations at any given range the positive separation distance will result in a different correlation to the

negative separation distance. For example, say we are considering the correlations for the observation located at 30-km range; the correlation with the 18-km observation (-12 -km separation) will have a smaller measurement volume whereas the observation at 42 km ($+12$ -km separation) will have a larger measurement volume. This is an important factor to consider when analyzing the along-beam correlation results. When plotting the along-beam correlation functions, it can appear as though the plot is incomplete for data at low elevation, far range, and high height (e.g., Figs. 10 and 11). This is a result of the range limit of the radar. For example, as depicted in

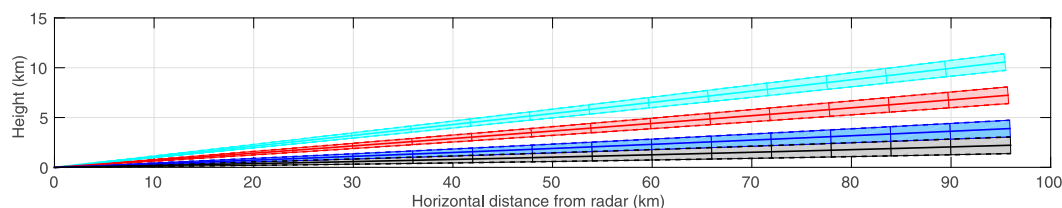


FIG. 2. A typical radar beam at elevations 1° (black), 2° (blue), 4° (red), and 6° (cyan).

TABLE 2. Horizontal and along-beam standard deviations calculated for cases 1–4 using all available data up to a height of 5 km.

Case	Horizontal standard deviation (m s^{-1})	Along-beam standard deviation (m s^{-1})
1	1.97	1.95
2	1.57	1.59
3	1.96	1.99
4	1.82	1.89

Fig. 2, at an elevation of 1° and height of 2.5 km, the range of the observation is 94 km. There are no observations available beyond a range of 100 km from the radar, so therefore we are unable to calculate the correlation beyond a separation distance of +6 km (i.e., 6 km farther from the radar).

For both horizontal and along-beam correlations it is possible to calculate an average correlation function using all available data that is homogeneous for all elevations, heights, and ranges. These average correlation functions provide an overall impression of how the calculated covariance differs between cases. The average along-beam correlation functions are also comparable to those calculated in Wattrelot et al. (2012). The disadvantage of this method is that different elevations represent different heights in the atmosphere, and also have interaction with different model levels. Therefore it is difficult to distinguish how the error correlations arise, whether they are a result of errors in the observation operator or arise from the misrepresentation of scales. In an attempt to understand exactly what is contributing to the error we also calculate the correlations for different elevations separately as this allows us to better understand the origin and behavior of the errors.

5. Results

a. Case 1—Results from the operational system

We begin by calculating the observation error covariances for case 1. Here data were acquired using the January 2014 operational system. This uses super-observations (calculated as described in section 3) thinned to 6 km, the observation operator given in (6), and the new background error covariance statistics.

1) HORIZONTAL CORRELATIONS

We first calculate the average horizontal correlation function using all data from all elevations. We show the standard deviation for this case in Table 2 and the correlation in Fig. 3. (Note that the table and figure contain results for all cases; in this section we discuss the results for case 1 only). The standard deviation falls within the range of operational DRW standard deviations. We see that the estimated correlation length scale [defined to be the distance at which correlation becomes insignificant (<0.2); Liu and Rabier 2002] is approximately 24 km. This is much larger than the distance of 1–3 km calculated in Simonin et al. (2012) using the method of Xu et al. (2007) and the operational thinning distance of 6 km. This indicates that the assumption of uncorrelated errors is incorrect.

We now consider the horizontal correlations for different heights and each elevation separately. In Fig. 4 we plot the standard deviation with height for each elevation. We see that the standard deviations increase with height, with the exception of the lowest levels, and are similar for each elevation. For each elevation, the volume of atmosphere sampled by the observation increases with height. (Note that at any given height the volume sampled by the 6° beam will be smaller than the 1° beam). Observations that sample larger volumes are

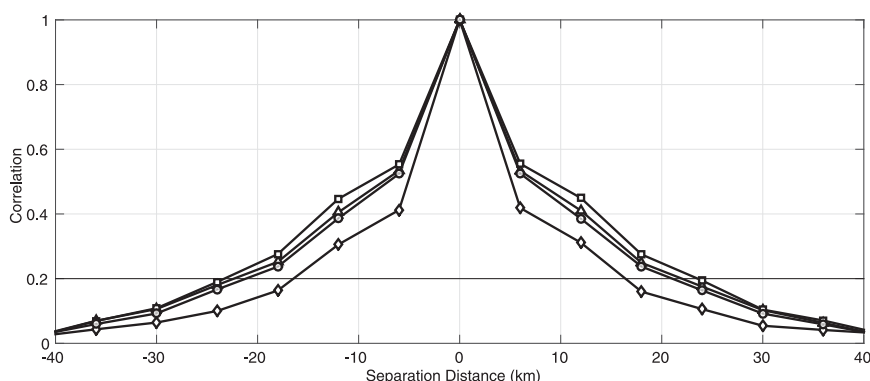


FIG. 3. All elevation horizontal observation error correlations for case 1 (control; squares), case 2 (alternate background error statistics; diamonds), case 3 (thinned raw data; triangles), and case 4 (new observation operator; circles). Error correlations are deemed to be insignificant below the horizontal line at 0.2.

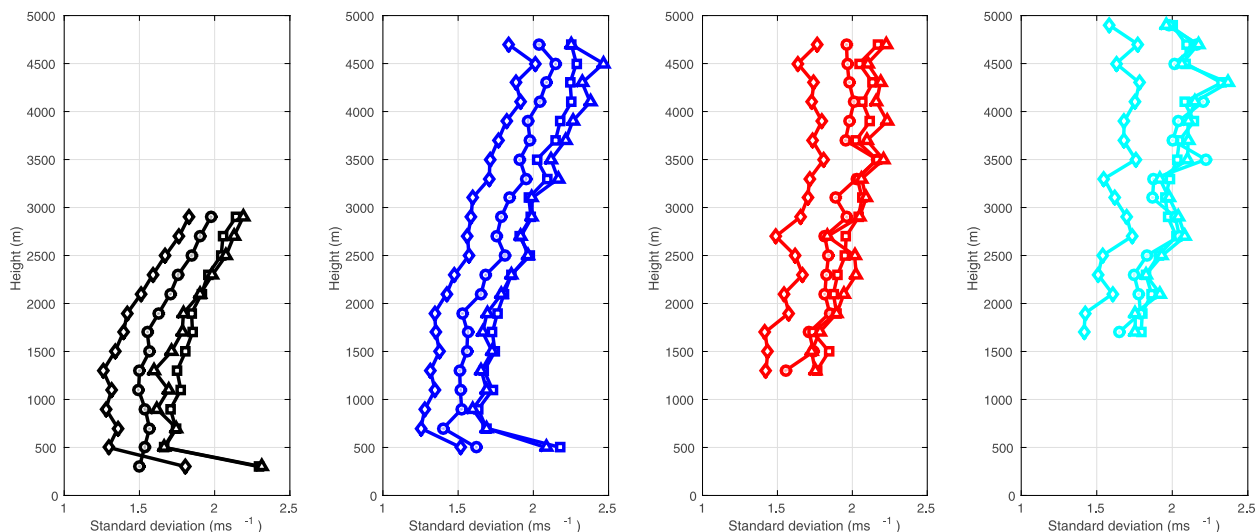


FIG. 4. Horizontal observation error standard deviation for elevations 1° (black), 2° (blue), 4° (red), and 6° (cyan) for case 1 (control; squares), case 2 (alternate background error statistics; diamonds), case 3 (thinned raw data; triangles) and case 4 (new observation operator; circles).

expected to have a larger instrument error as the Doppler shift is calculated from multiple scattering targets in the measurement volume. In addition, these observations will be subject to more error from the observation operator as only information from the model level nearest to the center of the sample volume is utilized, even when the sample volume spans several model layers. The increased errors at the lowest height may be a result of larger representativity errors as the observations at the lower heights sample smaller volumes than the model resolution. Our results support previous work in Simonin et al. (2014) and we find that the standard deviations are similar to those used operationally.

Next we consider how the horizontal correlation length scale changes for a given elevation at different heights. We plot the calculated correlation functions for a range of

heights in Fig. 5. We see that the correlation length scale increases with height and ranges between 17 and 32 km. For all heights the correlation length scale is longer than the operational thinning distance. An increase in height corresponds to an increase in both the distance of observation away from the radar and the volume of the measurement box and therefore the change in correlation length scale could be attributed to either of these variables.

In an attempt to determine the cause of the change in length scale we consider the horizontal correlations at the 2.5-km height for the different elevations. At any given height the measurement volume of the observation is larger for lower elevations. Figure 6 shows that the correlation length scales are larger for the lower elevations. This suggests that it is the change in measurement volume that affects the correlation length scale. As in this case the

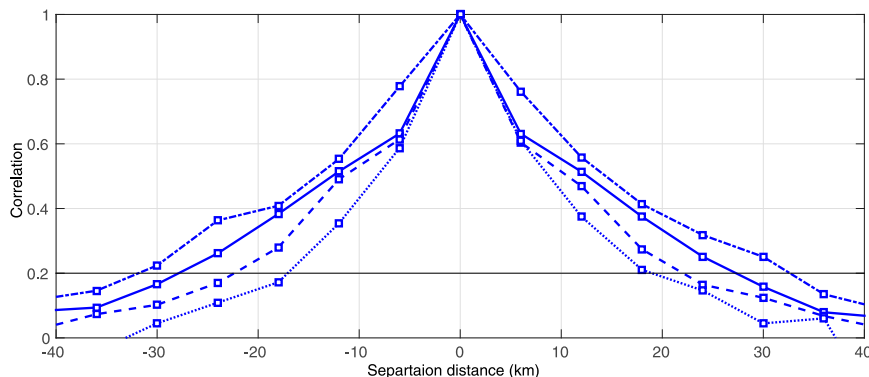


FIG. 5. Horizontal observation correlations for elevation 2° at heights 1.1 km (dotted), 2.7 km (dashed), 3.5 km (solid), and 4.3 km (dot-dashed) for case 1 (control). Error correlations are deemed to be insignificant below the horizontal line at 0.2.

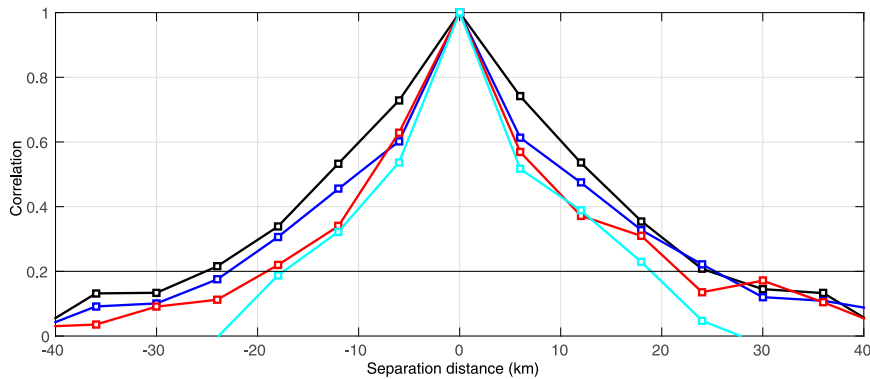


FIG. 6. Horizontal correlations at height 2.5 km for elevations 1° (black), 2° (blue), 4° (red), and 6° (cyan) for case 1 (control). Error correlations are deemed to be insignificant below the horizontal line at 0.2.

observation operator does not account for the observation volume, it is likely that the correlated error is, in part, caused by the error in the observation operator.

It is also possible to compare observations at the same range, observations will have the same measurement volume but will be at different heights in the atmosphere. In this case we find that for each elevation the correlation length scale is similar (e.g., at a range of 40 km each elevation has a correlation length scale of ~ 23 km; not shown). This suggests that the measurement volume of the observation has the largest impact on the horizontal correlation length scale, with correlation length scale increasing with measurement volume.

2) ALONG-BEAM CORRELATIONS

Next we calculate the along-beam observation errors using the data from case 1. We begin by calculating the

average observation error covariance and comparing these results with those from Météo-France (Wattrelet et al. 2012). We do not expect estimated statistics to be equal to those found by Météo-France as there are differences in the operational setup (e.g., observation and background error covariance statistics, observation processing, observation operators, and thinning distances) and the region and time scale covered by the data.

Our estimated standard deviation (Table 2) is larger than the standard deviation found by Météo-France, which is 1.51 m s^{-1} . This is likely to be the result of the different operational setup and observation processing. We plot our estimated correlation function along with the correlation found by Météo-France in Fig. 7. We see that the correlation length scales are approximately 5 km longer than those found by Météo-France. Given the different operational setup used by

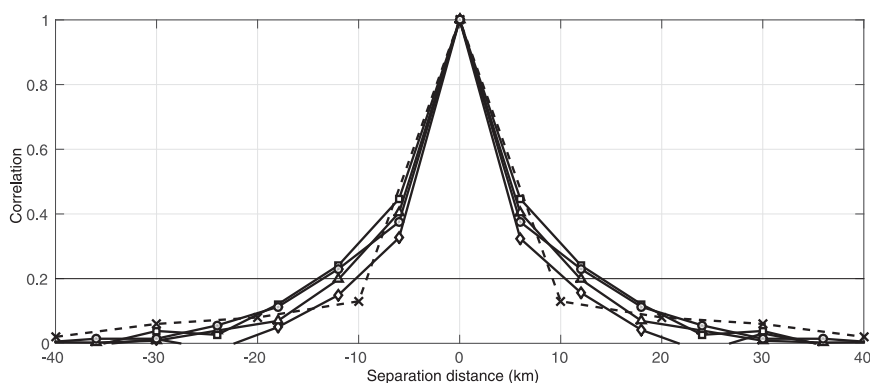


FIG. 7. All elevation along-beam observation error correlation for cases 1 (control; squares), 2 (alternate background error statistics; diamonds), 3 (thinned raw data; triangles), and 4 (new observation operator; circles) and those found previously by Météo-France (crosses). Error correlations are deemed to be insignificant below the horizontal line at 0.2.

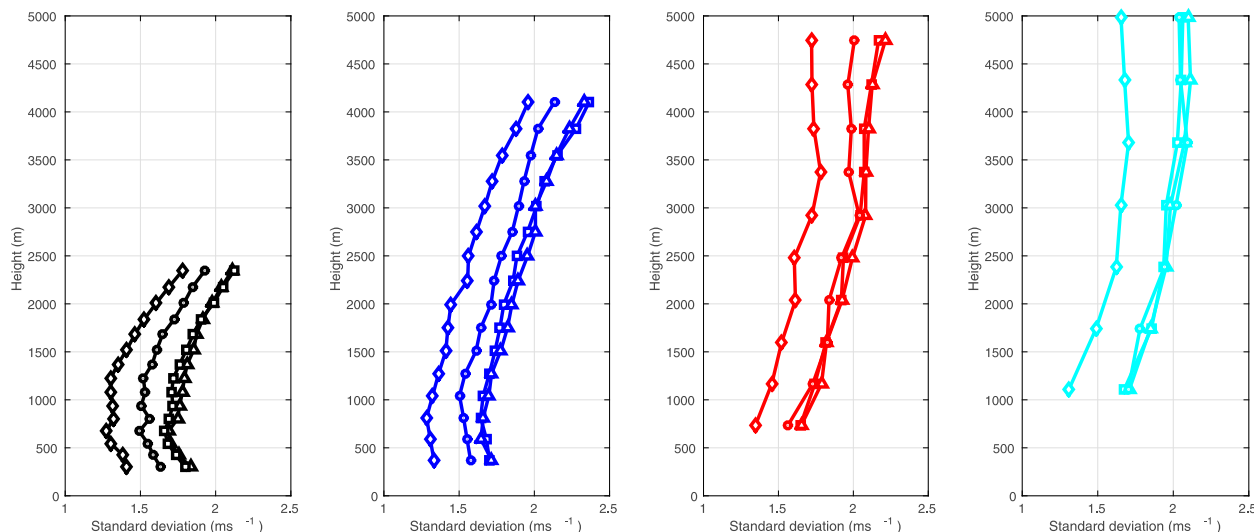


FIG. 8. Along-beam observation error standard deviation for elevations 1° (black), 2° (blue), 4° (red), and 6° (cyan) for case 1 (control; squares), case 2 (alternate background error statistics; diamonds), case 3 (thinned raw data; triangles), and case 4 (new observation operator; circles).

Météo-France, the similarities between the results are reassuring and suggest that we are obtaining a reasonable estimate of the observation error correlations.

Next we calculate the error statistics along the beam for each elevation. In Fig. 8 (square symbols) we plot the change in standard deviation with height for beam elevations of 1° , 2° , 4° , and 6° . (For the horizontal correlations the height of the radar above sea level was accounted for; here height is calculated assuming that the radar is at sea level). For all elevations the observation error standard deviation generally increases with height, with the exception of the lowest levels. This is similar to the behavior of the standard deviations for the horizontal case. Unlike the horizontal case the standard deviations for each elevation are not so similar. For any

given height the standard deviations are larger for the lower elevations. At any given height the lower elevations will be sampling larger volumes of the atmosphere. Observations sampling large volumes are subject to both larger instrument error and more error in the observation operator.

We now consider how the correlation length scale changes for a given elevation at different heights. The estimated observation error correlations for a range of heights are plotted in Fig. 9. The along-beam correlation length scales are shorter than the horizontal correlations, although the correlation length scale still increases with height for any given elevation. This highlights the relationship between the increase in correlation length scale with the increasing height, range, and volume measurement of the observation.

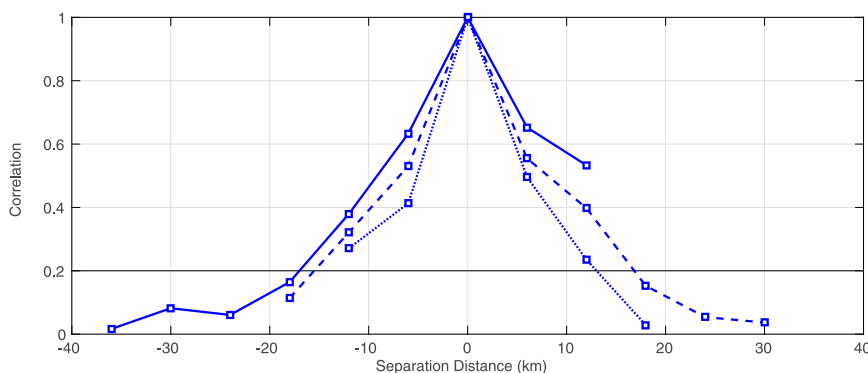


FIG. 9. Along-beam observation correlations for elevation 2° at heights 1.1 km (dotted), 3.0 km (dashed), and 3.5 km (solid) for case 1 (control).

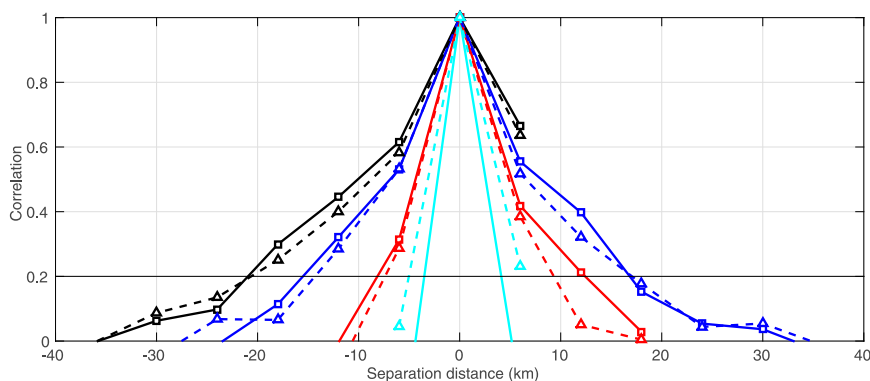


FIG. 10. Correlations along the beam at height 2.5 km for elevations and approximate ranges $1^\circ \approx 94$ km (black), $2^\circ \approx 64$ km (blue), $4^\circ \approx 35$ km (red), and $6^\circ \approx 22$ km (cyan) for superobbed data (squares/solid lines) and thinned raw data (triangles/dashed lines). Error correlations are deemed to be insignificant below the horizontal line at 0.2.

In Fig. 10 we consider how the correlation function differs with measurement volume. We plot the along-beam correlation function for each elevation at a height of 2.5 km. Here the height for each observation is the same, but the measurements are taken at different ranges with the lowest elevation at the farthest range. Figure 10 shows that the correlation length scale increases with range. Again this is likely to be a result of the larger measurement volumes at far range.

In Fig. 11 we plot the correlation function for each elevation at a range of 40 km. Here the volume of measurement for each observation is the same, but measurements from lower elevations are at lower heights. We see that the correlation length scale differs with elevation and decreases with height. We hypothesize that the change in correlation is a result of the different levels of the atmosphere sampled by different beam elevations.

For the low elevation angles the beam gradient is shallow, hence different gates measure similar heights in the atmosphere; this results in larger error correlations. Larger elevation angles have larger beam gradients, and different gates sample a wider range of heights in the atmosphere; this results in small observation error correlations.

3) SUMMARY

For this case we have calculated observation error statistics using background residuals from June, July, and August 2013, the analysis residuals are produced by running the UKV model using the January 2014 operational configuration. We find the following:

- DRW standard deviations increase with height (with the exception of the lowest heights). This is likely due

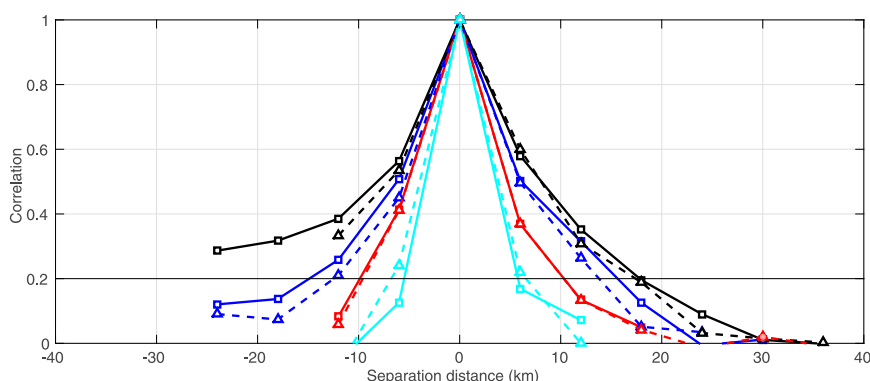


FIG. 11. Correlations along the beam at range 40 km for elevations and approximate heights $1^\circ \approx 0.8$ km (black), $2^\circ \approx 1.5$ km (blue), $4^\circ \approx 3.0$ km (red), and $6^\circ \approx 4.3$ km (cyan) for superobbed data (solid lines) and thinned raw data (dashed lines). Error correlations are deemed to be insignificant below the horizontal line at 0.2.

to the increasing measurement volume with height. The larger errors at the lowest height are likely to be a result of representativity errors.

- The correlation length scale is larger than the thinning distance of 6 km chosen to ensure that the assumption of uncorrelated errors is valid.
- For both horizontal and along-beam correlations and for all elevations the observation error correlation length scale increases with height. We hypothesize that this is in part due to the larger errors in the observation operator and correlated superobservation errors at large range. This will be the subject of further investigation (see sections 5c and 5d).

b. Case 2—The effect of changing the assimilated background error statistics

The diagnostic of Desroziers et al. (2005) uses the assumption that the observation and background error covariance matrices used in the assimilation are exact. In the operational assimilation, case 1, the observation errors are assumed uncorrelated and the background error variance and correlation length scale are believed to be too large. (The Met Office has an ongoing project to develop an improved background error covariance matrix; this is expected to reduce error variances and correlation length scales compared to those used in case 1 of this study.) Results given in Waller et al. (2016) relating to the diagnostic suggest that under these circumstances the diagnostic will underestimate the observation error correlation length scale. Therefore it is possible that the true observation error statistics have longer correlation lengths than those calculated for case 1.

To provide information on how results in case 1 may compare to the true observation error statistics, we consider the sensitivity of the estimated observation error statistics to using different background statistics. Here we use previous operational background error statistics that have larger variances and larger length scales than the background error statistics used in the previous experiments.

1) HORIZONTAL CORRELATIONS

The average standard deviation given in Table 2 shows that the use of background error statistics with larger variance and longer length scales results in a lower estimate of the observation error standard deviation. The correlation function, plotted in Fig. 3, shows clearly that using a different background error covariance matrix has reduced the estimated observation error correlation length scale. These results agree with

the theoretical results in Waller et al. (2016) (larger overestimates of variance and correlation length scale in the assimilated background statistics result in more severe underestimates of observation error variance and correlation length scale) and suggest that the theoretical results developed under simplifying assumptions are still applicable in an operational setting. The theoretical work and results from cases 1 and 2 suggest that if the variances and length scales in the assumed covariance matrix \mathbf{B} were further reduced compared to case 1, the estimated observation error correlation length scales would be larger.

Figure 4 shows that the change in standard deviation with height for each elevation is similar to case 1. However, the standard deviations for case 2 are smaller than those from case 1, a result of the larger background error variances used in the assimilation.

As with the average correlations, results relating to the correlations for each individual elevation and height have smaller correlation length scales than case 1 (not shown). However, we still find that the qualitative behavior of the correlation length scales remains the same; that is, for any elevation the correlation length scale increases with height and for any given height the length scale decreases as elevation increases.

2) ALONG-BEAM CORRELATIONS

For the average along-beam correlation we find the standard deviation (Table 2) is reduced compared to case 1. The correlations plotted in Fig. 7 also have a shorter length scale (approximately 10 km) and are more comparable to those found by Météo-France.

When considering the standard deviations for each elevation we again see that they are reduced (see diamonds in Fig. 8), although the change in standard deviation with height is qualitatively similar to case 1. We find that the shape of the correlation function is similar, but the length scales are shorter than those calculated in case 1 (not shown). The variation in the correlation length scale with elevation, height, and range is, however, unaltered.

3) SUMMARY

For this case we have calculated observation error statistics using different background error statistics that have larger variances and correlation length scales. We find the following:

- Estimated observation error standard deviations (length scales) are smaller (shorter) when using the alternative background error statistics with larger standard deviations and longer correlation length

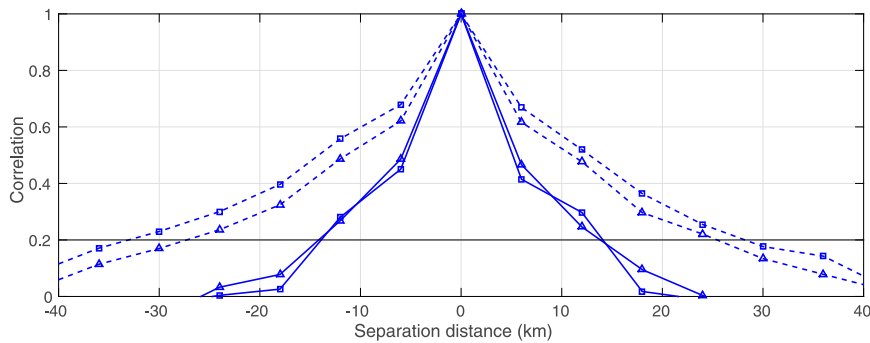


FIG. 12. Horizontal observation correlations for elevation 2° at a range of 24 km (solid) and 90 km (dashed) for case 1 (control; squares) and case 3 (thinned raw data; triangles). Error correlations are deemed to be insignificant below the horizontal line at 0.2.

scales. This result follows the theoretical work of Waller et al. (2016).

- Changes in observation error standard deviation and correlation length scale with height remain qualitatively similar to case 1.
- Given that the background error standard deviations and correlation length scales in case 1 are believed to be too large and long, it is likely that the true observation error statistics have larger standard deviations and longer length scales than those calculated in case 1.

c. Case 3—The effect of the superobservations

The creation of the superobservations, discussed in section 3b, results in an observation error that is only independent of the background error if the errors in the background states used in the calculation of each superobservation are of the same magnitude and are fully correlated (Berger and Forsythe 2004). This assumption is true at close range to the radar, but it is possible that it is violated at far range resulting in increased observation error correlation length scales. To determine if the superobservations have this effect we consider the results from case 3, where the assimilation uses thinned raw data. We return to using the new background error statistics.

1) HORIZONTAL CORRELATIONS

Table 2 shows that the average standard deviation for this case is very similar to that of case 1. However, the correlation length scale is slightly reduced compared to case 1 (Fig. 3). This suggests that the use of superobservations may introduce some observation error correlation but does not appear to be the main source of correlations.

Figure 4 shows that the standard deviations for individual elevations are similar to those found in case 1. In general we find that the use of the thinned data results in slightly shorter observation error correlation length

scales for observations that are at lower elevations and far range. For example, Fig. 12 shows, for the 2° elevation, that the use of the superobservations has little impact on the correlation length scale at short range. However, at far range the correlation length scale for case 1 is approximately 5 km longer than that for case 3. This result supports our hypothesis that the use of superobservations increases the observation error correlation length scale at far range. This is a result of the invalid assumption that the errors in the background states used in the superobservation creation are of the same magnitude and fully correlated.

2) ALONG-BEAM CORRELATIONS

From Table 2 we see that the average along-beam observation error standard deviation is similar to that found using the data from case 1. Figure 7 shows that the correlation length scale is also slightly reduced.

Figure 8 shows that the standard deviations for separate elevations are similar to case 1. Figures 10 and 11 show that using the raw observations results in a similarly shaped correlation function to case 1 but with a slightly reduced length scale. The exception is the highest elevation (closest range) where the length scales are slightly larger. These results suggest that using the superobservation has the opposite effect, namely the introduction of correlation at far range, but a reduction of correlation in the higher elevations.

3) SUMMARY

We have calculated observation error statistics using thinned raw observations. We make these findings:

- Using thinned raw data has little impact on the estimated observation error standard deviations; this is similar to case 1.
- In general, horizontal correlation length scales at far range are reduced. This implies that using super-

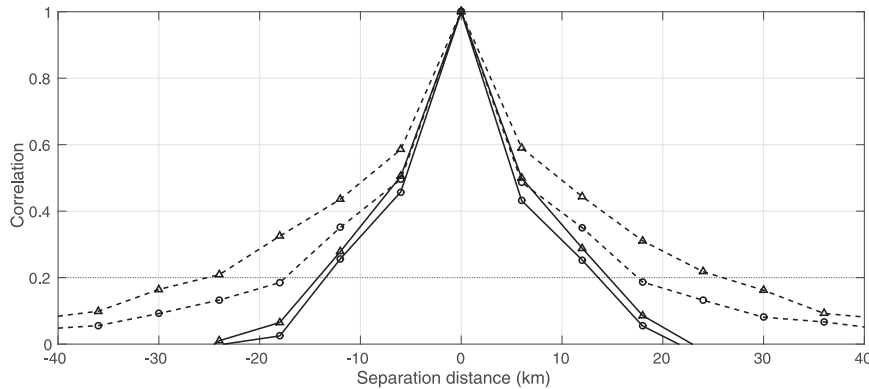


FIG. 13. Horizontal observation correlations for elevation 1° at a range of 18 km (solid) and 74 km (dashed) for case 3 (thinned raw data; triangles) and case 4 (new observation operator; circles). Error correlations are deemed to be insignificant below the horizontal line at 0.2.

observations introduces correlated error at far range, possibly as a result of an invalid assumption in the superobservation creation.

- In general along-beam correlation length scales are reduced for the lower elevations; however, they are slightly increased for the 6° beam.
- d. *Case 4—The effect of an improved observation operator*

The previous cases have all used the simplified observation operator described in (6). The omission of the more complex terms introduces both additional error variance and correlation (Fabry 2010). It may not be possible to use a full observation operator in operational assimilation, although the use of the sophisticated observation operator in (11) may be considered. In this case we use this new observation operator to see if including beam broadening and reflectivity weighting in the observation operator has any effect on the observation error statistics. Here we use the thinned raw observations rather than the superobservations (the creation of the superobservation involves the observation operator, and ideally we wish to isolate the impact of the observation operator in the assimilation), so the results here must be compared to case 3.

1) HORIZONTAL CORRELATIONS

For the average horizontal error statistics both the standard deviation and correlation length scale have decreased compared to case 3 (see Table 2 and Fig. 3).

For the separate elevations, as with all previous cases, we find that the standard deviations increase with height (Fig. 4), although here the actual values for the lower elevations are reduced compared to the standard deviations found in case 3. The reduction is not seen in the higher elevations as observations are at near range

where the effects of beam bending and broadening, accounted for in the new observation operator, are not so significant. In general, we find that the correlations for every elevation are decreased when using the improved observation operator. In Fig. 13 we show that using an improved observation operator reduces the correlation length scale slightly at near range, and at far range by approximately 40%.

When considering horizontal correlations we compare observations at the same range away from the radar that have the same measurement volume, and hence the new observation operator should have the same improvement for each observation we compare. The reduction in error standard deviation and correlation shows that the inclusion of the beam broadening and reflectivity weighting has improved the observation operator. It also suggests that the use of an even more sophisticated observation operator may further reduce the observation error correlation.

2) ALONG-BEAM CORRELATIONS

In this case Table 2 and Fig. 8 show that the error standard deviation is reduced compared to case 3, suggesting that the more sophisticated observation operator is indeed an improved map from background to observation space. Both Fig. 7 and the correlations for separate elevations suggest that introducing the new observation operator slightly increases the correlation length scale. We hypothesize that this is a result of the inclusion of the beam broadening. When using the old observation operator observations at different ranges at any elevation were unlikely to consider data from the same model levels. With the introduction of the beam broadening different observations will now use information from the same model levels and this is

likely to be the cause of the increased correlation length scales.

3) SUMMARY

For this case we have calculated observation error statistics using thinned raw observations and an improved observation operator. We find the following:

- Using the new observation operator reduces the error standard deviations for the lower elevations. Less impact is seen in the higher elevations where the effects of beam bending and broadening (accounted for in the new observation operator) are not so significant.
- For the horizontal correlations using the new observation operator reduces the estimated observation correlation length scale. This suggests that error in the observation operator may be in part responsible for the large correlation length scales.
- Using the new observation operator increases the along-beam correlation. This is likely to be the result of close observation residuals sharing increased amounts of background data.

6. Conclusions

With the development of convection-permitting NWP the assimilation of high-resolution observations is becoming increasingly important. Currently large quantities of high-resolution data are discarded to ensure the assumption of uncorrelated observation errors is reasonable. The assimilation of high-resolution observations will require less thinning of the observational data and, hence, the inclusion of correlated observation error statistics in the assimilation system. Observation errors can be attributed to a number of different sources, some of which may be state dependent and dependent on the model resolution. Calculation of observation error statistics is difficult as they cannot be measured directly. Recently the diagnostic of [Desroziers et al. \(2005\)](#) has been used to estimate interchannel observation error correlations for a number of different observation types. When inexact background and observation errors are used in the assimilation cost function, theory ([Waller et al. 2016](#)) shows that the results arising from the diagnostic are uncertain and should be interpreted as indicative, rather than necessarily quantitatively perfect. However, results from the diagnostics can still provide useful information on the sources of error correlation and how it may be reduced. Furthermore, idealized studies using correlated observation error matrices indicate that much of the benefit in assimilation accuracy can be obtained from using approximate correlation structures ([Stewart et al. 2013](#); [Healy and White 2005](#)).

The aim of this manuscript is to use the diagnostic to estimate spatially correlated errors for Doppler radar radial wind (DRW) observations that are assimilated into the Met Office UKV model. Errors for DRWs may be correlated horizontally, vertically, or along the path of the radar beam. In this work we consider both the horizontal and along-beam error statistics. We also considered if results from the [Hollingsworth and Lönnerberg \(1986\)](#) diagnostic could provide further information. We note that, for the data used in this study, there was no clear way to partition the results from the [Hollingsworth and Lönnerberg \(1986\)](#) diagnostic into the observation and background error portions. Any observation error correlations estimated from this data using the [Hollingsworth and Lönnerberg \(1986\)](#) method would have been highly dependent on the subjective choice of correlation function fitted.

Initially error statistics were calculated for observations assimilated into the UKV model operational in January 2014. This provided information on the general structure of the observation errors and how they vary throughout the atmosphere. Error statistics were also calculated using data from an assimilation run using alternative background error statistics. This provided information on how sensitivity of the results to the specification of the background error statistics. The diagnostic was then applied to data from two additional assimilation runs. These evaluated the impact that the use of superobservations and errors in the observation operator has on the estimated observation error statistics.

Results from all four cases showed similar behavior for the estimated statistics. We are able to conclude that most DRW error standard deviations and horizontal and along-beam correlation length scales increase with height, as a function of the increase in measurement volume. Thus at least part of the correlated error is likely to be related to the uncertainty in the observation operator. The exceptions are the standard deviations at the lowest heights. Observations at the lowest heights have the smallest measurement volumes, smaller than the model grid spacing, and hence representativity errors may well account for the larger standard deviations at lower heights. The results presented here are for summer season observations; however, results considered for winter season observations show that the qualitative behavior of the estimated DRW error statistics is similar to the summer case.

Results showed that the estimated standard deviations are similar to those used operationally. However for the majority of cases, with exception of the 6° beam, the correlation length scales are much larger than those found in [Simonin et al. \(2012\)](#) and the operational thinning distance of 6 km. Despite the differences in operational system, our estimated average along-beam

correlations are similar to those calculated by Météo-France (Wattrelot et al. 2012). Furthermore, observation error statistics estimated when using an alternative background error covariance matrix in the assimilation and the results from Waller et al. (2016) imply that the observation error correlation length scale is underestimated. This suggests that the errors are correlated to a degree that it should be accounted for in the assimilation.

In an attempt to understand the source of the error correlations, the effects of using superobservations and an improved observation operator are considered. The use of the superobservations does not affect the error standard deviations. However, results suggest that the use of superobservations introduces correlated error at far range, possibly as a result of an invalid assumption in the superobservation creation. The use of an improved observation operator reduces the error standard deviations, particularly at low elevations and at far range where observations have large measurement volumes. This is expected since the new observation operator takes into account the beam broadening and bending, both of which affect the beam most at far range. The improvement in the low elevations is related to the inclusion in the observation operator of information from more model levels. These are denser in the lower atmosphere where the low elevations provide observations. The use of the new observation operator results in an increase of the along-beam correlation length scale. We hypothesize that this is a result of nearby observation residuals now sharing information from the same model levels. However, the horizontal correlations were slightly reduced. This suggests not only that some of the horizontal correlations previously seen were a result of omissions in the observation operator, but also that the horizontal correlation length scale may be further reduced with the use of an even more complex observation operator.

These results provide a better understanding of DRW observation error statistics and the sources that contribute to them. We have shown that these observation errors exhibit large spatial correlations that are much larger than the operational thinning distance. This implies that, if high-resolution DRW observations are to be assimilated correctly, the inclusion of correlated observation error statistics in the assimilation system is required.

Acknowledgments. This work is funded in part by the NERC Flooding from Intense Rainfall programme (NE/K008900/1) and the NERC National Centre for Earth Observation. We also thank the two anonymous reviewers whose comments were greatly appreciated. The data used in this study may be obtained on request, subject to licensing conditions, by contacting the corresponding author.

REFERENCES

- Ballard, S. P., Z. Li, D. Simonin, and J.-F. Caron, 2016: Performance of 4D-Var NWP-based nowcasting of precipitation at the Met Office for summer 2012. *Quart. J. Roy. Meteor. Soc.*, **142**, 472–487, doi:10.1002/qj.2665.
- Berger, H., and M. Forsythe, 2004: Satellite wind superobbing. Met Office Forecasting Research Tech. Rep. 451, 33 pp.
- Bondarenko, V., T. Ochotta, and D. Saupe, 2007: The interaction between model resolution, observation resolution and observations density in data assimilation: A two-dimensional study. *11th Symp. on Integrated Observing and Assimilation Systems for the Atmosphere, Oceans, and Land Surface*, San Antonio, TX, Amer. Meteor. Soc., P5.19. [Available online at <http://ams.confex.com/ams/pdfpapers/117655.pdf>.]
- Bormann, N., and P. Bauer, 2010: Estimates of spatial and inter-channel observation-error characteristics for current sounder radiances for numerical weather prediction. I: Methods and application to ATOVS data. *Quart. J. Roy. Meteor. Soc.*, **136**, 1036–1050, doi:10.1002/qj.616.
- , A. Collard, and P. Bauer, 2010: Estimates of spatial and inter-channel observation-error characteristics for current sounder radiances for numerical weather prediction. II: Application to AIRS and IASI data. *Quart. J. Roy. Meteor. Soc.*, **136**, 1051–1063, doi:10.1002/qj.615.
- Clark, P., N. Roberts, H. Lean, S. Ballard, and C. Charlton-Perez, 2015: Convection-permitting models: A step-change in rainfall forecasting. *Meteor. Appl.*, **23**, 165–181, doi:10.1002/met.1538.
- Courtier, P., J. Thépaut, and A. Hollingsworth, 1994: A strategy for operational implementation of 4D-Var, using an incremental approach. *Quart. J. Roy. Meteor. Soc.*, **120**, 1367–1387, doi:10.1002/qj.49712051912.
- Dance, S. L., 2004: Issues in high resolution limited area data assimilation for quantitative precipitation forecasting. *Physica D*, **196**, 1–27, doi:10.1016/j.physd.2004.05.001.
- Dee, D. P., and A. M. da Silva, 1999: Maximum-likelihood estimation of forecast and observation error covariance parameters. Part I: Methodology. *Mon. Wea. Rev.*, **127**, 1822–1834, doi:10.1175/1520-0493(1999)127<1822:MLEOFA>2.0.CO;2.
- Desroziers, G., L. Berre, B. Chapnik, and P. Poli, 2005: Diagnosis of observation, background and analysis-error statistics in observation space. *Quart. J. Roy. Meteor. Soc.*, **131**, 3385–3396, doi:10.1256/qj.05.108.
- Doviak, R. J., and D. S. Zrnić, 1993: *Doppler Radar and Weather Observations*. 2nd ed. Academic Press, 592 pp.
- Fabry, F., 2010: Radial velocity measurement simulations: Common errors, approximations, or omissions and their impact on estimation accuracy. *Proc. Sixth European Conf. on Radar in Meteorology and Hydrology*, Sibiu, Romania, ERAD, 17.2.
- , and A. Kilambi, 2011: The devil is in the details: Preparing radar information for its proper assimilation. *35th Conf. on Radar Meteorology*, Pittsburgh, PA, Amer. Meteor. Soc., 19A.6. [Available online at <https://ams.confex.com/ams/35Radar/webprogram/Paper191698.html>.]
- Ge, G., J. Gao, K. Brewster, and M. Xue, 2010: Impacts of beam broadening and Earth curvature on 3D variational radar data assimilation with two Doppler radars. *J. Atmos. Oceanic Technol.*, **27**, 617–636, doi:10.1175/2009JTECHA1359.1.
- Hand, W. H., N. I. Fox, and C. G. Collier, 2004: A study of twentieth-century extreme rainfall events in the United Kingdom with implications for forecasting. *Meteor. Appl.*, **11**, 15–31, doi:10.1017/S1350482703001117.

- Hawcroft, M. K., L. C. Shaffrey, K. I. Hodges, and H. F. Dacre, 2012: How much Northern Hemisphere precipitation is associated with extratropical cyclones? *Geophys. Res. Lett.*, **39**, L24809, doi:[10.1029/2012GL053866](https://doi.org/10.1029/2012GL053866).
- Healy, S. B., and A. A. White, 2005: Use of discrete Fourier transforms in the 1D-Var retrieval problem. *Quart. J. Roy. Meteor. Soc.*, **131**, 63–72, doi:[10.1256/qj.03.193](https://doi.org/10.1256/qj.03.193).
- Hollingsworth, A., and P. Lönnberg, 1986: The statistical structure of short-range forecast errors as determined from radiosonde data. Part I: The wind field. *Tellus*, **38A**, 111–136, doi:[10.1111/j.1600-0870.1986.tb00460.x](https://doi.org/10.1111/j.1600-0870.1986.tb00460.x).
- Janjić, T., and S. E. Cohn, 2006: Treatment of observation error due to unresolved scales in atmospheric data assimilation. *Mon. Wea. Rev.*, **134**, 2900–2915, doi:[10.1175/MWR3229.1](https://doi.org/10.1175/MWR3229.1).
- Kitchen, M., 1997: Towards improved radar estimates of surface precipitation rate at long range. *Quart. J. Roy. Meteor. Soc.*, **123**, 145–163, doi:[10.1002/qj.49712353706](https://doi.org/10.1002/qj.49712353706).
- Lean, H., P. Clark, M. Dixon, N. Roberts, A. Fitch, R. Forbes, and C. Halliwell, 2008: Characteristics of high-resolution versions of the Met Office Unified Model for forecasting convection over the United Kingdom. *Mon. Wea. Rev.*, **136**, 3408–3424, doi:[10.1175/2008MWR2332.1](https://doi.org/10.1175/2008MWR2332.1).
- Lindskog, M., H. Jarvinen, and D. B. Michelson, 2000: Assimilation of radar radial winds in the HIRLAM 3D-Var. *Phys. Chem. Earth*, **25B**, 1243–1249, doi:[10.1016/S1464-1909\(00\)00187-8](https://doi.org/10.1016/S1464-1909(00)00187-8).
- , and Coauthors, 2001: Three-dimensional variational data assimilation for a limited area model. Part II: Observation handling and assimilation experiments. *Tellus*, **53A**, 447–468, doi:[10.1111/j.1600-0870.2001.00447.x](https://doi.org/10.1111/j.1600-0870.2001.00447.x).
- , K. Salonen, H. Jarvinen, and D. B. Michelson, 2004: Doppler radar wind assimilation with HIRLAM 3DVAR. *Mon. Wea. Rev.*, **132**, 1081–1092, doi:[10.1175/1520-0493\(2004\)132<1081:DRWDAW>2.0.CO;2](https://doi.org/10.1175/1520-0493(2004)132<1081:DRWDAW>2.0.CO;2).
- Liu, Z.-Q., and F. Rabier, 2002: The interaction between model resolution observation resolution and observation density in data assimilation: A one-dimensional study. *Quart. J. Roy. Meteor. Soc.*, **128**, 1367–1386, doi:[10.1256/003590002320373337](https://doi.org/10.1256/003590002320373337).
- , and —, 2003: The potential of high-density observations for numerical weather prediction: A study with simulated observations. *Quart. J. Roy. Meteor. Soc.*, **129**, 3013–3035, doi:[10.1256/qj.02.170](https://doi.org/10.1256/qj.02.170).
- Lorenc, A. C., and Coauthors, 2000: The Met Office global three-dimensional variational data assimilation scheme. *Quart. J. Roy. Meteor. Soc.*, **126**, 2991–3012, doi:[10.1002/qj.49712657002](https://doi.org/10.1002/qj.49712657002).
- Montmerle, T., and C. Faccani, 2009: Mesoscale assimilation of radial velocities from Doppler radars in a preoperational framework. *Mon. Wea. Rev.*, **137**, 1939–1953, doi:[10.1175/2008MWR2725.1](https://doi.org/10.1175/2008MWR2725.1).
- Park, S. K., and D. Zupanski, 2003: Four-dimensional variational data assimilation for mesoscale and storm-scale applications. *Meteor. Atmos. Phys.*, **82**, 173–208, doi:[10.1007/s00703-001-0586-7](https://doi.org/10.1007/s00703-001-0586-7).
- Piccolo, C., and M. Cullen, 2011: Adaptive mesh method in the Met Office variational data assimilation system. *Quart. J. Roy. Meteor. Soc.*, **137**, 631–640, doi:[10.1002/qj.801](https://doi.org/10.1002/qj.801).
- , and —, 2012: A new implementation of the adaptive mesh transform in the Met Office 3D-Var system. *Quart. J. Roy. Meteor. Soc.*, **138**, 1560–1570, doi:[10.1002/qj.1880](https://doi.org/10.1002/qj.1880).
- Rawlins, F., S. P. Ballard, K. J. Bovis, A. M. Clayton, D. Li, G. W. Inverarity, A. C. Lorenc, and T. J. Payne, 2007: The Met Office global four-dimensional variational data assimilation scheme. *Quart. J. Roy. Meteor. Soc.*, **133**, 347–362, doi:[10.1002/qj.32](https://doi.org/10.1002/qj.32).
- Rennie, S. J., A. J. Illingworth, S. L. Dance, and S. P. Ballard, 2010: The accuracy of Doppler radar wind retrievals using insects as targets. *Meteor. Appl.*, **17**, 419–432, doi:[10.1002/met.174](https://doi.org/10.1002/met.174).
- , S. L. Dance, A. J. Illingworth, S. P. Ballard, and D. Simonin, 2011: 3D-Var assimilation of insect-derived Doppler radar radial winds in convective cases using a high-resolution model. *Mon. Wea. Rev.*, **139**, 1148–1163, doi:[10.1175/2010MWR3482.1](https://doi.org/10.1175/2010MWR3482.1).
- Rihan, F. A., C. G. Collier, S. P. Ballard, and S. J. Swarbrick, 2008: Assimilation of Doppler radial winds into a 3D-Var system: Errors and impact of radial velocities on the variational analysis and model forecasts. *Quart. J. Roy. Meteor. Soc.*, **134**, 1701–1716, doi:[10.1002/qj.326](https://doi.org/10.1002/qj.326).
- Salonen, K., H. Jarvinen, R. Eresmaa, and S. Niemelä, 2007: Bias estimation of Doppler radar radial-wind observations. *Quart. J. Roy. Meteor. Soc.*, **133**, 1501–1507, doi:[10.1002/qj.114](https://doi.org/10.1002/qj.114).
- , —, S. Jarvenoja, S. Niemelä, and R. Eresmaa, 2008: Doppler radar radial wind data in NWP model validation. *Meteor. Appl.*, **15**, 97–102, doi:[10.1002/met.47](https://doi.org/10.1002/met.47).
- , —, G. Haase, S. Niemelä, and R. Eresmaa, 2009: Doppler radar radial winds in HIRLAM. Part II: Optimizing the super-observation processing. *Tellus*, **61A**, 288–295, doi:[10.1111/j.1600-0870.2008.00381.x](https://doi.org/10.1111/j.1600-0870.2008.00381.x).
- Simonin, D., S. Ballard, Z. Li, and J. F. Caron, 2012: Doppler radar assimilation. *Proc. 27th European Conf. on Radar in Meteorology and Hydrology*, Toulouse, France, ERAD, 24 pp. [Available online at <http://www.meteo.fr/cic/meetings/2012/ERAD/presentations/friday/14-2.pdf>.]
- , S. P. Ballard, and Z. Li, 2014: Doppler radar radial wind assimilation using an hourly cycling 3D-Var with a 1.5 km resolution version of the Met Office Unified Model for nowcastings. *Quart. J. Roy. Meteor. Soc.*, **140**, 2298–2314, doi:[10.1002/qj.2298](https://doi.org/10.1002/qj.2298).
- Stewart, L. M., 2010: Correlated observation errors in data assimilation. Ph.D. thesis, University of Reading, 195 pp. [Available online at <http://www.reading.ac.uk/math-and-stats/research/theses/math-phdtheses.aspx>.]
- , S. L. Dance, and N. K. Nichols, 2008: Correlated observation errors in data assimilation. *Int. J. Numer. Methods Fluids*, **56**, 1521–1527, doi:[10.1002/fld.1636](https://doi.org/10.1002/fld.1636).
- , J. Cameron, S. L. Dance, S. English, J. R. Eyre, and N. K. Nichols, 2009: Observation error correlations in IASI radiance data. University of Reading Tech. Rep., 26 pp. [Available online at www.reading.ac.uk/web/FILES/math/obs_error_IASI_radiance.pdf.]
- , S. L. Dance, and N. K. Nichols, 2013: Data assimilation with correlated observation errors: Experiments with a 1-D shallow water model. *Tellus*, **65A**, 19546, doi:[10.3402/tellusa.v65i0.19546](https://doi.org/10.3402/tellusa.v65i0.19546).
- , —, —, J. R. Eyre, and J. Cameron, 2014: Estimating interchannel observation-error correlations for IASI radiance data in the Met Office system. *Quart. J. Roy. Meteor. Soc.*, **140**, 1236–1244, doi:[10.1002/qj.2211](https://doi.org/10.1002/qj.2211).
- Sun, J., 2005: Convective-scale assimilation of radar data: Progresses and challenges. *Quart. J. Roy. Meteor. Soc.*, **131**, 3439–3463, doi:[10.1256/qj.05.149](https://doi.org/10.1256/qj.05.149).
- , and Coauthors, 2014: Use of NWP for nowcasting convective precipitation: Recent progresses and challenges. *Bull. Amer. Meteor. Soc.*, **95**, 409–426, doi:[10.1175/BAMS-D-11-00263.1](https://doi.org/10.1175/BAMS-D-11-00263.1).
- Tang, Y., H. W. Lean, and J. Bornemann, 2013: The benefits of the Met Office variable resolution NWP model for forecasting convection. *Meteor. Appl.*, **20**, 417–426, doi:[10.1002/met.1300](https://doi.org/10.1002/met.1300).
- Toomay, J., and P. Hannen, 2004: *Radar Principles for the Non Specialist*. 3rd ed. SciTech Publishing, 267 pp.

- Waller, J. A., 2013: Using observations at different spatial scales in data assimilation for environmental prediction. Ph.D. thesis, Department of Mathematics and Statistics, University of Reading, 132 pp. [Available online at <http://www.reading.ac.uk/math-and-stats/research/theses/math-phdtheses.aspx>.]
- , S. L. Dance, A. S. Lawless, and N. K. Nichols, 2014a: Estimating correlated observation error statistics using an ensemble transform Kalman filter. *Tellus*, **66A**, 23294, doi:[10.3402/tellusa.v66.23294](https://doi.org/10.3402/tellusa.v66.23294).
- , —, —, —, and J. R. Eyre, 2014b: Representativity error for temperature and humidity using the Met Office high-resolution model. *Quart. J. Roy. Meteor. Soc.*, **140**, 1189–1197, doi:[10.1002/qj.2207](https://doi.org/10.1002/qj.2207).
- , —, and N. K. Nichols, 2016: Theoretical insight into diagnosing observation error correlations using observation-minus-background and observation-minus-analysis statistics. *Quart. J. Roy. Meteor. Soc.*, **142**, 418–431, doi:[10.1002/qj.2661](https://doi.org/10.1002/qj.2661).
- Wattrelot, E., T. Montmerle, and C. G. Guerrero, 2012: Evolution of the assimilation of radar data in the AROME model at convective scale. *Proc. Seventh European Conf. on Radar in Meteorology and Hydrology*, Toulouse, France, ERAD. [Available online at www.meteo.fr/cic/meetings/2012/ERAD/extended_abs/NWP_401_ext_abs.pdf.]
- Weston, P. P., W. Bell, and J. R. Eyre, 2014: Accounting for correlated error in the assimilation of high-resolution sounder data. *Quart. J. Roy. Meteor. Soc.*, **140**, 2420–2429, doi:[10.1002/qj.2306](https://doi.org/10.1002/qj.2306).
- Xiao, Q., and Coauthors, 2008: Doppler radar data assimilation in KMAs operational forecasting. *Bull. Amer. Meteor. Soc.*, **89**, 39–43, doi:[10.1175/BAMS-89-1-39](https://doi.org/10.1175/BAMS-89-1-39).
- , Y.-H. Kuo, J. Sun, W.-C. Lee, E. Lim, Y.-R. Guo, and D. M. Barker, 2005: Assimilation of Doppler radar observations with a regional 3DVAR system: Impact of Doppler velocities on forecasts of a heavy rainfall case. *J. Appl. Meteor.*, **44**, 768–788, doi:[10.1175/JAM2248.1](https://doi.org/10.1175/JAM2248.1).
- Xu, Q., and L. Wei, 2013: Prognostic equation for radar radial velocity derived by considering atmospheric refraction and Earth curvature. *J. Atmos. Sci.*, **70**, 3328–3338, doi:[10.1175/JAS-D-13-011.1](https://doi.org/10.1175/JAS-D-13-011.1).
- , K. Naib, and L. Wei, 2007: An innovation method for estimating radar radial-velocity observation error and background wind error covariances. *Quart. J. Roy. Meteor. Soc.*, **133**, 407–415, doi:[10.1002/qj.21](https://doi.org/10.1002/qj.21).
- Xue, M., F. Kong, K. Thomas, J. Gao, Y. Wang, K. Brewster, and K. Droegemeier, 2013: Prediction of convective storms at convection-resolving 1-km resolution over continental United States with radar data assimilation: An example case of 26 May 2008 and precipitation forecasts from spring 2009. *Adv. Meteor.*, **2013**, 259052, doi:[10.1155/2013/259052](https://doi.org/10.1155/2013/259052).
- , M. Hu, and A. Schenkman, 2014: Numerical prediction of 8 May 2003 Oklahoma City tornadic supercell and embedded tornado using ARPS with assimilation of WSR-88D radar data. *Wea. Forecasting*, **29**, 39–62, doi:[10.1175/WAF-D-13-00029.1](https://doi.org/10.1175/WAF-D-13-00029.1).